Interdecadal changes in interannual variability of the global monsoon precipitation and interrelationships among its subcomponents

Eun-Jeong Lee · Kyung-Ja Ha · Jong-Ghap Jhun

Abstract The interdecadal and the interannual variability of the global monsoon (GM) precipitation over the area which is chosen by the definition of Wang and Ding (Geophys Res Lett 33: L06711, 2006) are investigated. The recent increase of the GM precipitation shown in previous studies is in fact dominant during local summer. It is evident that the GM monsoon precipitation has been increasing associated with the positive phase of the interdecadal Pacific oscillation in recent decades. Against the increasing trend of the GM summer precipitation in the Northern Hemisphere, its interannual variability has been weakened. The significant change-point for the weakening is detected around 1993. The recent weakening of the interannual variability is related to the interdecadal changes in interrelationship among the GM subcomponents around 1993. During P1 (1979–1993) there is no significant interrelationship among GM subcomponents. On the other hand, there are significant interrelationships among the Asian, North American, and North African summer monsoon precipitations during P2 (1994–2009). It is noted that the action center of the interdecadal changes is the Asian summer (AS) monsoon system. It is found that during P2 the Western North Pacific summer monsoon (WNPSM)-related variability is dominant but during P1 the ENSO-related variability is dominant over the AS monsoon region. The WNPSM-related variability is rather related to central-Pacific (CP) type ENSO rather than the eastern-Pacific (EP) type ENSO. Model experiments confirm that the CP type ENSO forcing is related to the dominant WNPSM-related variability and can be responsible for the significant interrelationship among GM subcomponents.

Keywords Global monsoon · Western North Pacific summer monsoon · Interdecadal change · Precipitation · Interdecadal Pacific oscillation · CP warming

1 Introduction

The monsoon is a forced response of the coupled atmosphere–ocean–land system, which is phase-locked in an annual cycle. Monsoon climate studies have focused on regional monsoons because of their indigenous characteristics due to the specific land–ocean configurations, different atmosphere–ocean–land interactions, and considerable regionality of monsoon variations. To fully understand changes in regional monsoons, a global perspective is required. The global monsoon (GM) system is a persistent global-scale overturning of the atmosphere that varies according to the time of year (Trenberth et al. 2000). Wang and Ding (2006) proposed a simple metrics of the GM and defined its subcomponents including Asian, Australian, North/South American, and North/South African monsoon systems.

Climate disasters arising from GM precipitation changes and variabilities can influence agriculture, water resources, energy, economy, and society. Thus, understanding the interannual-to-interdecadal variability and long-term changes of the GM and its subcomponents is of particular importance. Due to lack of observations over ocean, the GM precipitation cannot be fully studied until recently. Wang and Ding (2006) recognized that the GM

E.-J. Lee · K.-J. Ha (✉)
Division of Earth Environmental System,
Pusan National University, Pusan, Korea
e-mail: kjha@pusan.ac.kr

J.-G. Jhun
School of Earth and Environmental Sciences/Research Institute
of Oceanography, Seoul National University, Seoul, Korea

precipitation over land decreased from 1950 to 1980 but leveled off after 1980. However, the satellite estimate of oceanic monsoon rainfall indicates an increasing trend over the recent three decades (Wang and Ding 2006) which has increased the total GM rainfall (Wang et al. 2012; Hsu et al. 2011). Several progresses have been made after Wang and Ding (2006). For example, Zhou et al. (2008a) has investigated the changes of global and regional monsoon area and monsoon precipitation. They find that the monsoon weakening identified by Wang and Ding (2006) was mainly dominated by North African and Asian monsoon. In addition to total monsoon precipitation changes, global monsoon area has also changed. Zhang and Zhou (2011) has studied twentieth century changes of global and regional land monsoon precipitation. They find that the weakening of global monsoon is only evident in the past 50 years. In the early part of the twentieth century the global monsoon precipitation exhibited an increasing trend. Recently, Lee and Wang (2012) showed that the recent intensification is larger in the NH than SH and suggested that the NH monsoon precipitation will continuously increase during twenty-first century under the anthropogenic global warming but the SH will not.

Interannual to interdecadal variabilities of the GM subcomponents have received much attention, particularly for the Asian-Australian monsoon system (e.g., Wang et al. 2003, 2008 and many others) and East Asia—the Western North Pacific monsoon system (e.g., Kwon et al. 2005; Yun et al. 2010 and many others). Also, the GM has been a useful metric for gauging the performance of climate models. Zhang et al. (2010) evaluated the performance of a coupled general circulation model in simulating the annual modes of tropical precipitation. Kitoh et al. (2013) investigated a regional monsoon perspective in a global context using future climate scenario data. Regarding the linkage among subsystems of the wide Asian-Australian monsoon, some papers have clearly studied the inter-monsoon connections. The South Asian monsoon and the Australian monsoon circulations are better reproduced than the others (Zhou et al. 2009). Interconnected monsoon variabilities to the Asian-Australian in East Asia, Indochina, and the Western North Pacific are investigated (Zhou et al. 2011). However, for the GM system, inter-monsoon connections over global scale have not been studied. In order to better understand recent and future changes of the GM system, important questions to be addressed include how the GM subcomponents are related each other in interannual time scale and how the interrelationship changes in interdecadal time scale. Understanding of feedback processes between the GM subcomponents may provide a key to capture the predictive source of climate change.

The objective in this study is to examine interdecadal changes in the hemispheric monsoon systems and interrelationships among the GM subcomponents during recent three decades. The rest of this paper is organized in the following manner. Section 2 introduces observational data and methods used in the present study. In Sect. 3, the interdecadal variability of hemispheric monsoons and their large-scale drivers are investigated. Also, changes in interrelationships and dominant spatial patterns among precipitations in the GM subcomponents are given in Sect. 3. Possible causes and experimental results are addressed in Sect. 4. Section 5 contains a summary and discussion.

2 Data, analysis methods and model experiments

2.1 Observational datasets

By using the Global Precipitation Climatology Project (GPCP) version 2.2 monthly combined precipitation data from 1979 to 2003 with a horizontal resolution of 2.5° by 2.5°, recorded by the World Climate Research Program (WCRP) (Adler et al. 2003), Wang and Ding (2006) defined a global monsoon domain and detected an increasing trend in global monsoon rainfall. With the same analysis method, Zhou et al. (2008b) explained oceanic monsoon rainfall by using the GPCP, the CPC Merged Analysis of Precipitation (CMAP), and the Special Sensor Microwave Imager (SSM/I) during 1979–2000. They found robust increasing trends for the GPCP and SSM/I but a weak decreasing trend for the CMAP. For global precipitation analysis, the GPCP and the CMAP datasets are widely used. From both datasets, the global monsoon intensity has a consistent downward trend, but changes in land and oceanic global monsoon intensity have opposite signs because changes depend on the contribution from the land monsoon in the GPCP and from the oceanic monsoon in the CMAP. Over the ocean, the trends are opposite because of different algorithms in both datasets, the inconsistency of the GPCP and the CMAP data is mainly located over the ocean area. Compared two observation datasets, it is suggested that the GPCP precipitation data are probably more reliable than those than the CMAP precipitation data through comparing to other data source (Zhou et al. 2008b; Hsu et al. 2011).

For this reason, the GPCP version 2.2 data from 1979 to 2010 has been used as observational precipitation data. This data covers both land and ocean and is combined with rain gauge data and the satellite estimates. In addition, the Hadley Centre Global Sea Surface Temperature (HadISST) dataset (Rayner et al. 2003), acquired by the British Atmospheric Data Centre, covers only oceans with a horizontal resolution of 1.0° by 1.0°. For geopotential heights at 850 and 500 hPa, surface winds reported by the National Centers for Environmental Prediction–National Center for

Atmospheric Research (NCEP–NCAR) reanalysis dataset (Kalnay et al. 1996), which has a horizontal resolution of 2.5° by 2.5°, have been used to examine changes related to the WNPSM.

2.2 Global monsoon definition

Previous studies defined global monsoon domains by using different datasets, several of which are listed in Table 1. Little differences among definitions are shown in bold. Wang and Ding (2006) used the ensemble mean of the four datasets and GPCP precipitation data to define a region in which the annual range (AR, the local summer minus following winter) exceeds 180 mm and the local summer monsoon precipitation exceeds 35 % of annual rainfall. In Wang and Ding (2008), the monsoon domain is defined by an AR exceeding 300 mm and a Monsoon Precipitation Index (MPI) exceeding 0.5. Liu et al. (2009) defined a global monsoon region in which the AR of precipitation rate exceeds 2 mm per day and the local summer monsoon precipitation exceeds 55 % of annual rainfall. Wang and Ding (2008) and Liu et al. (2009) used extended summer and winter data to determine annual range. The slightly different criteria actually show similar results in global monsoon domain.

In the present study, which uses the Wang and Ding (2006) definition, global monsoon domains are delineated as shown in Fig. 1. Hereafter, June–July–August (JJA) refers to the summer in the Northern Hemisphere (NH) and the winter in the Southern Hemisphere (SH), and December–January–February (DJF) refers to the opposite. By definition, global monsoon domains include six regional monsoon domains—Northern African (NAF), Asian (AS), Northern American (NAM), Southern African (SAF), Australian (AU), and Southern American (SAM)—that exhibit the land–ocean thermal contrast. The NAF, AS, and NAM domains are located in the NH, while the SAF, AU, and SAM monsoon domains in the SH. Unlike the others, the AS domain ranges from the tropics to the mid-latitudes.

## 2.3 Detection of change-point and model experiment

Parametric and non-parametric tests are frequently used for change-point deduction. The parametric procedure generally uses the maximum likelihood ratio test and requires distribution of the data (Chen and Gupta 2000). Since the precipitation datasets only cover a short time period and are highly variable, the careful analysis is required to obtain the information of statistical significance. Because the precipitation data does not allow for the determination of appropriate distribution to describe the data, the non-parametric changing point test, which does not use the distribution of the data, has been used. Ha and Ha (2006) divided the entire period of the precipitation at Seoul into three subperiods by using the test statistics of Pettitt (1979). This study uses Lepage and Pettitt test to detect change-point ("Appendix").

To examine the effects of SST forcing over the eastern Pacific (EP) and central Pacific (CP) on reproducibility of global monsoon precipitation during 2 periods, the European Community–Hamburg model (ECHAM) version 4.6 is performed, which is a global spectral model that includes triangular truncation at waver number 42 and a 19-level hybrid sigma-pressure coordinate system. The nonlinear terms and the parameterized physical processes were calculated on a 128° by 64° Gaussian grid, with a horizontal resolution of about 2.8° by 2.8°. Model details may be found in Roeckner et al. (2003).

Table 1 Data sets and definitions of global monsoon domain used in previous studies

	Data sets	Definitions of global monsoon domain
Wang and Ding (2006)	Delaware (1950–1999), PREC/L (1948–2003), VASCO (1951–2000), and CRU (1948–2002) data → Ensemble mean of the four data sets (1948–2003) + GPCP data (1979–2003)	Region in which the annual range (AR) of precipitation exceeds **180 mm** and the local summer monsoon precipitation exceeds **35 %** of annual rainfall
		AR: **JJA minus DJF** in Northern Hemisphere or **DJF minus JJA** in Southern Hemisphere
Wang and Ding (2008)	CMAP, NECP2, ERA40, and JRA25(1979–2007) data	Region in which the annual range (AR) of precipitation exceeds **300 mm** and the MPI (Monsoon Precipitation Index) exceeds **0.5**
		AR: **MJJAS minus NDJFM** in Northern Hemisphere or **NDJFM minus MJJAS** in Southern Hemisphere
Liu et al. (2009)	CMAP data	Region in which the annual range (AR) of precipitation rate exceeds **2 mm/day** and the local summer monsoon precipitation exceeds **55 %** of annual rainfall
		AR: **MJJAS minus NDJFM** in Northern Hemisphere or **NDJFM minus MJJAS** in Southern Hemisphere

Fig. 1 Global monsoon domains defined according to Wang and Ding (2006) using recent precipitation data
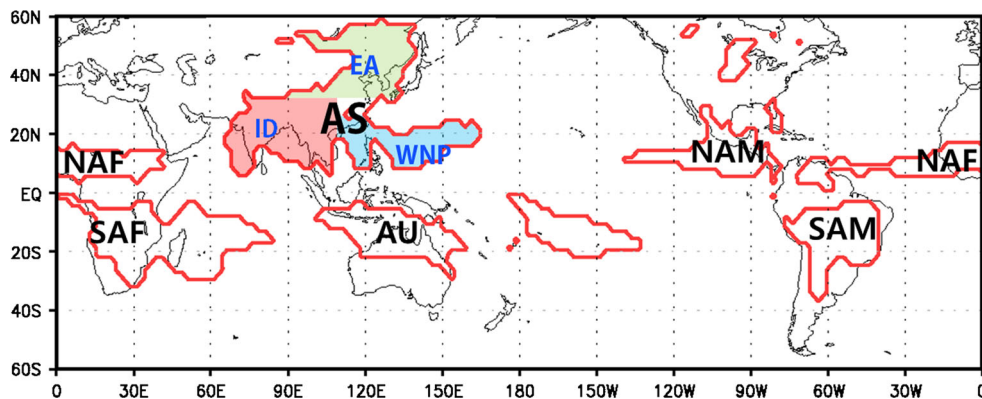
3 Distinct interdecadal changes

3.1 Trend and interannual variability of the GM summer precipitation

We further investigate long-term trend of the GM precipitation in the NH and the SH given the fact that the GM precipitation particularly in the NH has been increasing during recent 30 years (Wang et al. 2012; Lee and Wang 2012). It is noted that the monsoon precipitation is increasing during local summer but decreasing during local winter. During local summer, trends are 4.278 mm 92 days^{-1} 31 years^{-1} over the NH and 16.182 mm 90 days^{-1} 31 years^{-1} over the SH. During local winter, trends are -2.79 mm 90 days^{-1} 31 years^{-1} over the NH and -9.4116 mm 92 days^{-1} 31 years^{-1} over the SH. The increasing trend of summer monsoon precipitation may cause more heavy rainfall events during summer monsoon period.

Along with the summer monsoon intensification, there are interdecadal changes in interannual variability of the GM precipitation in the NH and SH during local summer. It is found that the two hemispheric GM summer precipitations have different interdecadal changes in their interannual variability. While the interannual variability of the summer precipitation in the NH has been weakened, that in the SH has increasing trend during recent three decades (Fig. 2a, b). It can make confusion between the weakening of variability and weakening of magnitude. In fact, the weakening of the NH monsoon has been noted in several previous studies (Wang and Ding 2006; Zhou et al. 2008a; Zhang and Zhou 2011). However, we focus the weakening of variability that related to the fluctuation, but not the weakening of monsoon intensity. In particular, the weakening of the NH monsoon variability is very significant. The sliding variance with 7-year window for the NH precipitation variability indicates that there is a statistically significant change-point around 1993 (Fig. 2c).

To determine drivers for the interdecadal hemispheric change, we have examined the sliding correlation between the NH summer monsoon precipitation and SST anomalies during the summer (Fig. 3). Since the sliding window is 15 years, for the period 1979–1993 and the center year is 1986, for example (Fig. 3a). As time progresses, the positive correlation over the WNP is weakened, and the negative correlation, which has the shape of a horseshoe, begins to appear in the center year of 1990. From the mid-1990s, a positive correlation appears over the eastern Pacific, and a negative correlation appears over the southern Pacific; this spatial pattern resembles an interdecadal Pacific oscillation (IPO) pattern over the entire Pacific basin. For this reason, SST is determined as a driver for the interdecadal change in the interannual variability of the NH GM summer precipitation. The driving of PDO or IPO-related SST to global monsoon has been demonstrated by Zhou et al. (2008b) based on numerical experiments. The external forcing may also have contributions (Li et al. 2010).

3.2 Interrelationship among GM subcomponents

Figure 2c and Lepage and Pettitt test indicate that the significant decadal change is detected around 1993. Thus, the entire data period is separated into P1 (1979–1993) and P2 (1994–2009) and we examine whether the interrelationship among GM subcomponents is changed between two epoch. A time series of the summer precipitation and schematic diagrams of relationships among the three NH monsoon precipitations during P1 and P2 are shown in Fig. 4. During P1, no significant correlations among precipitations are apparent over the three NH monsoon domains. Correlation coefficients of NAF–AS (r = 0.04), AS–NAM (r = -0.01) and NAF–NAM (r = 0.22) are not significant. However, stronger correlations revealed during P2 indicate that NAM and NAF have the same phase each other and that AS has opposite phases to NAF and NAM. All correlations are significant at the 95 % confidence level during P2. As stated above, the NAM and NAF monsoon precipitation are positively correlated (r = 0.44) and AS is

Fig. 2 The variability of precipitation over **a** the Northern Hemisphere (NH) and **b** the southern hemisphere (SH) monsoon domains in each summer. The sliding variance of precipitation over the NH monsoon domain is shown in **c**. The window in **c** is 7 years. A *vertical dashed line* indicates the year of the change-point
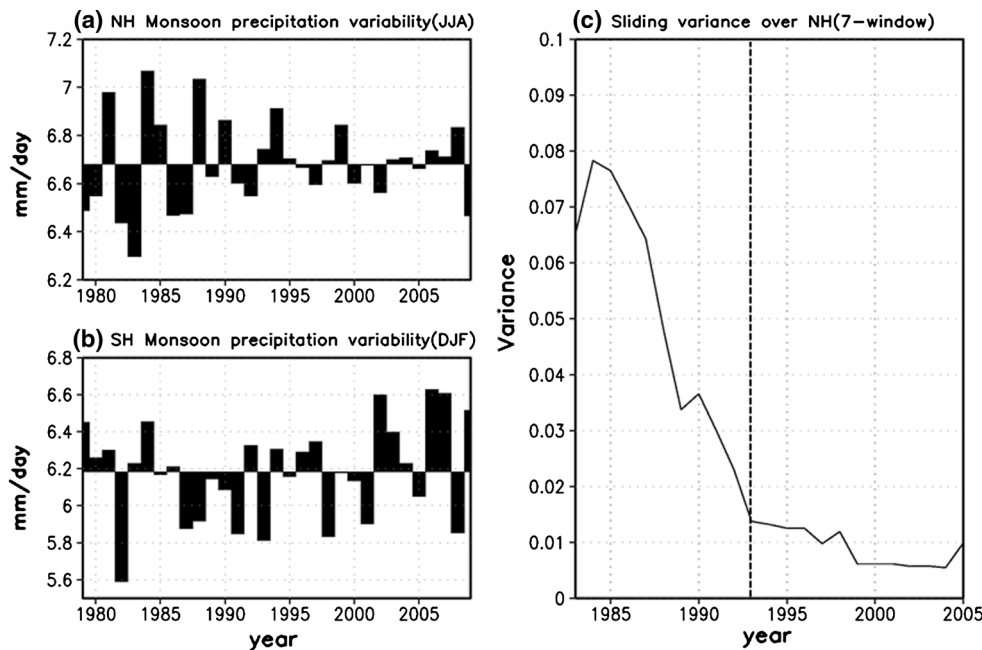
negatively correlated with NAM (r = −0.75) and NAF (r = −0.52). This indicates that precipitations over three NH monsoon domains are cancelled each other out to result in a weakening of monsoon precipitation variability during P2 (Fig. 2a).

The AS monsoon precipitation is thus negatively related to the others of NH monsoon precipitations, implying that the AS monsoon is an important component for changes in relationships among regional monsoon precipitation. The AS monsoon domain can be divided into three sub-regional monsoon domains: Indian (ID), East Asian (EA), and Western North Pacific (WNP) monsoon domains. The ID and WNP domains are located in the low latitudes, while the EA domain is in the mid-latitudes. The correlation coefficients between sub-regional and the AS precipitation are changed from 0.37 to 0.37 (ID-AS), 0.53 to −0.56 (EA-AS), and 0.84 to 0.78 (WNP-AS) during P1 and P2. Thus, the variability in the AS monsoon may be most related to that in the WNP monsoon during both P1 and P2, and the change in WNP seems to be related to that over the NH monsoon as well. For a global perspective, relationships among regional monsoon precipitations are summarized, as shown by the map in Fig. 5. In this map, the red belt indicates positive relationships among monsoon precipitations, which includes the NAM, NAF, and AU. On the contrary, blue solid lines indicate that some regional monsoon precipitations have negative relationships with AS monsoon precipitation, especially the WNPSM precipitation. It implies that WNPSM is a key factor for decadal changes in relationships among regional monsoon precipitations. The WNPSM has a negative correlation with NAF (−0.67), AU (−0.67), and NAM (−0.65).

3.3 Changes in spatial patterns of leading modes

Since changes have been identified in the relationships among NH monsoon precipitations, changes in dominant patterns for precipitation are examined by using the empirical orthogonal function (EOF) analysis over NAM, NAF, and AS monsoon domains for the two periods.

The first leading EOF mode over the region of the AS monsoon domain (0–60°N and 60°E–170°E) is shown in Fig. 6a, b. The variances of first mode account for about 21 and 30 % of the total variance during P1 and P2, respectively. In spatial distribution, a strong signal over WNPSM is apparent during the two periods. During P1, the correlation between the PC time series of the first mode (PC1) and the Niño 3.4 index is about 0.75, implying that the first mode is an ENSO-related mode. The correlation between the second mode PC time series (PC2) and the WNPSM index (Wang et al. 2001) is 0.77, indicating that the second mode is a WNPSM-related mode. During P2, the first mode is WNPSM-related mode and the correlation between PC1 and the WNPSM index is 0.98. The spatial pattern of the first mode during P2 is similar to that of the second mode during P1 (figure not shown). The dominant spatial pattern over the AS region is changed from the ENSO-related to the WNPSM-related mode. Although the AS domain in our study is larger than the East Asian domain studied by Kwon et al. (2005), changes in the most dominant mode are consistent with their results. In a previous study, the stationary wave-like pattern in the mid-latitudes associated with the convective activity over the WNP extended from East Asia to Alaska via northeastern China, Korea, and northern Japan (Wang et al. 2001). They argued that East

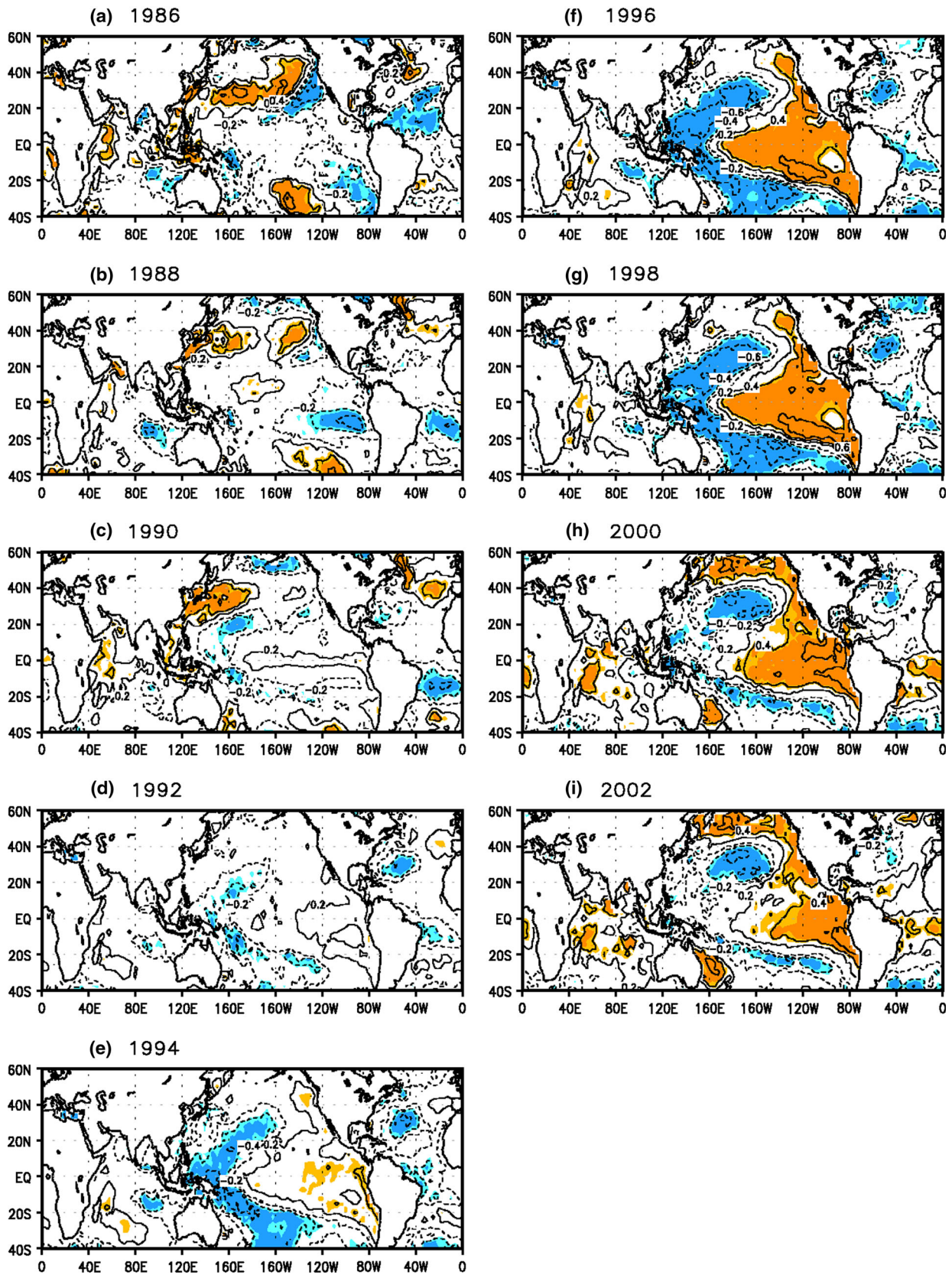Sliding Corr between decadal variability and JJA SST anomaly

(a) 1986

(b) 1988

(c) 1990

(d) 1992

(e) 1994

(f) 1996

(g) 1998

(h) 2000

(i) 2002

Asia has experienced a mean circulation change in the summertime since the mid-1990s (Kwon et al. 2005).

For the NAM domain, the bulk of monsoon moisture is transported at low levels from the eastern tropical Pacific and the Gulf of California, while the Gulf of Mexico may have contributed some moisture at upper levels (Adams and Comrie 1997). The dominant modes of this monsoon precipitation also changed during the two periods (figure not shown). The variance account of the first mode increases a little from 32.1 % during P1 to 32.6 % during P2. However, the pattern of first EOF mode during P1 has become the second EOF mode (19 %) during P2. The PC time series of these modes are related to the WNPSM and the correlation coefficients with the WNPSM index is changed from the positive value (0.46) during P1 to the negative value (−0.61) during P2. The variance in this mode and the magnitude of the signal near the boundary of land and ocean are weakened. Although the NAM monsoon is strongly related to the Pacific SST, it is also related to the WNPSM. Both the NAM and the WNPSM are driven by ENSO-related SST anomalies at interannual time scale. It is clear in the spectra of regional monsoon indicies as shown in Zhou et al. (2008a). We can summarize that the most dominant mode is the WNPSM mode during P1, but this WNPSM-related mode during P2 is less dominant in the NAM domain. Finally, for the NAF domain, changes of spatially dominant mode are investigated with the comparison for 2 periods in the same methods. We found that the first mode of the NAF monsoon pattern is stationary. However, the second and third modes have been reversed each other during P2. The second modes during

P1 and P2 are strongly correlated with the ISM and Niño 3.4 indices at the correlation coefficients of −0.46 and 0.72, respectively. These results imply that the dominant spatial patterns in global monsoon domains have been changed significantly from P1 to P2.

Changes in the relationship between the PC time series of the most dominant mode of the AS monsoon precipitation and SST over the Pacific Ocean have been detected. This AS monsoon can be divided into three regional monsoons: ID, WNP, and EA monsoons. Among these three regional monsoons, the WNPSM is most related to the AS summer monsoon. Because the AS-related SST pattern shows changes from the EP-related mode to CP-related mode, it is necessary to examine whether the relationship between the WNPSM and the SST pattern exhibits a decadal change as well. To examine which climate variables affects the change in the WNPSM, sliding correlations with other climate variables and indices have been calculated.

Figure 7 shows the sliding correlation pattern of summer SST anomalies with the WNPSM precipitation with a sliding window period of 15 years at the two-year interval. The year in the Fig. 7 indicates the central year of the window and the window period covers 7 years before and 7 years after the central year. For example, the central year in Fig. 7a is 1986 and thus the window includes 1979–1993. During this period, the WNPSM is negatively related to the Indian and the eastern Pacific Ocean SSTs and positively to the western Pacific and the northern Pacific Ocean SSTs, as shown in Fig. 7a. After 1994, correlation with the Indian Ocean and East Asia have been weakened, the WNPSM has positive relations with the central equatorial Pacific and the northern Pacific SST anomalies, as shown in Fig. 7f–i. Before 1993, the year of the change-point, the negative–positive–negative tripole-like structure is revealed over the Indian Ocean–western

Fig. 4 a Time series of summer (JJA) precipitation rate over NAF (*green*), AS (*red*), NAM (*blue*), and the NH (*black*) and **b** schematic diagrams showing relationships among JJA precipitations over regional monsoon domains during P1 (*left*) and P2 (*right*). *Red* and *blue lines* in **b** represent positive and negative correlations, respectively
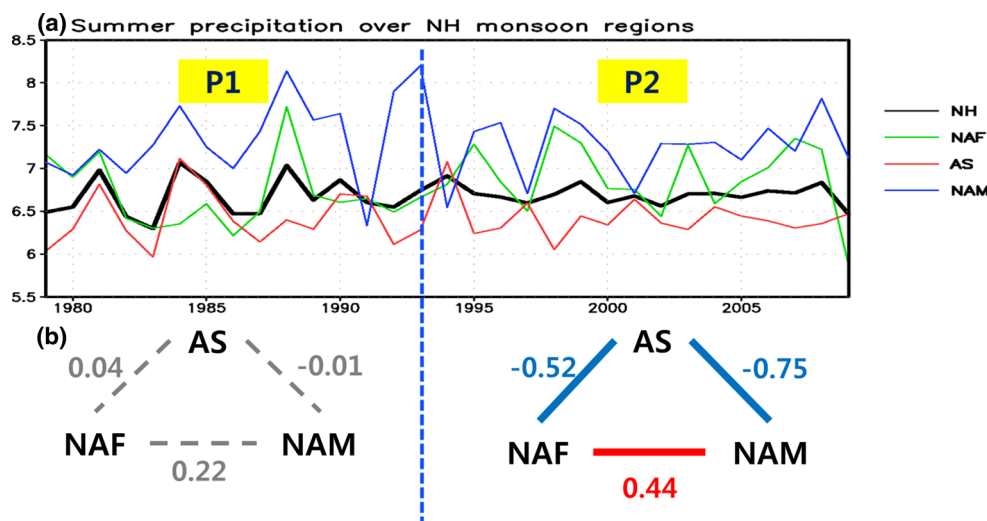
Pacific–eastern equatorial Pacific and northern Atlantic Ocean. As time goes on, the negative correlation over the Indian Ocean weakens, and the dipole structure of negative correlation over the WP and positive over the CP becomes evident. Figure 8 shows the sliding correlations between WNPSM (JJA) indices and six-month lagged SST anomalies (D(0)JF(+1)). During P1, positive and negative correlations are present over the northern Pacific and the equatorial Atlantic Oceans, respectively. However, during P2, a positive relationship is dominant over the Indian and the central equatorial Pacific Oceans, and a negative relationship appears over the western Pacific Ocean.

These relationships of the WNPSM (JJA) with simultaneous summer and six-month lagged winter SST anomalies show some characteristics of change. During P1, the correlation over the Indian Ocean is negative in the

summer and disappears in the following winter. However, during P2, a negative relationship was weakens in the summer and a positive relationship appears in the following winter over the Indian Ocean. Over the CP, a positive relationship appears in the summer and persists and strengthens until the following winter during P2. These two types of ENSO also have different teleconnections with the Indian Ocean. The EP La Niña-like pattern is strongly linked with the tropical Indian Ocean during the summer of P1, while the CP El Niño-like pattern is strongly associated with the southern Indian Ocean during the winter of P2.

Fig. 5 The map showing the relationship among regional summer monsoon precipitations in P2. The *red belt* indicates positive correlations one another. *Blue solid lines* denote negative relations with AS. The AU summer monsoon precipitation in the following D(0)JF(+1) is used to calculate the correlation coefficient
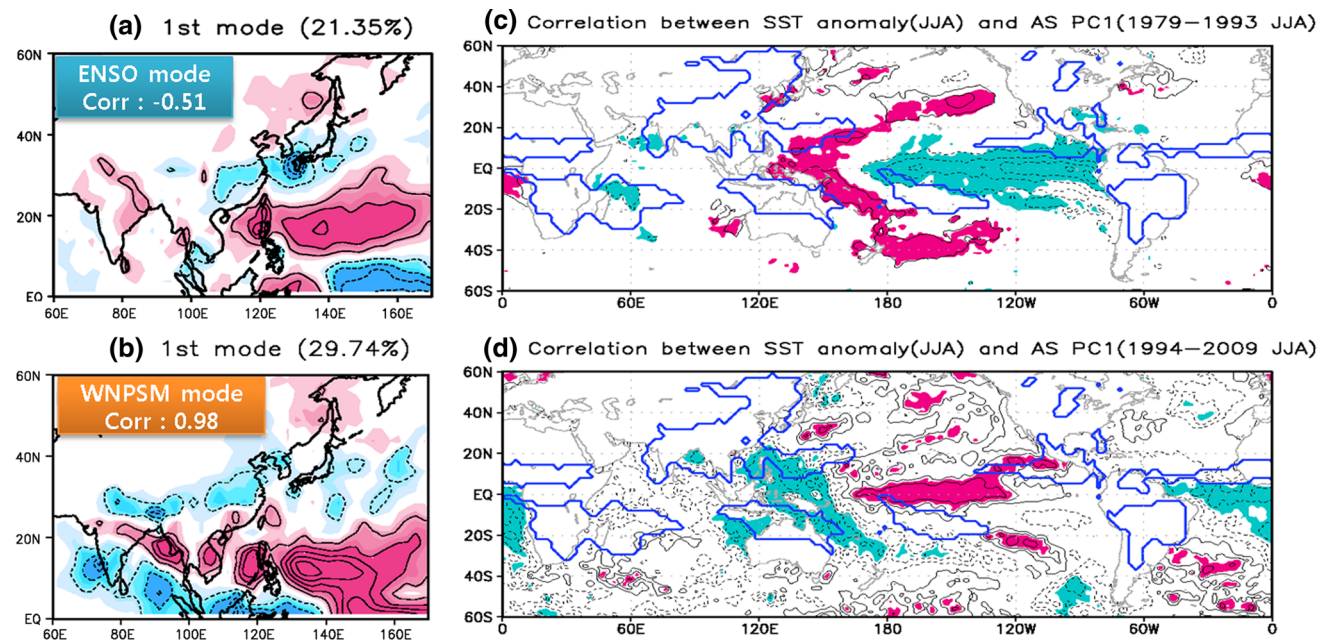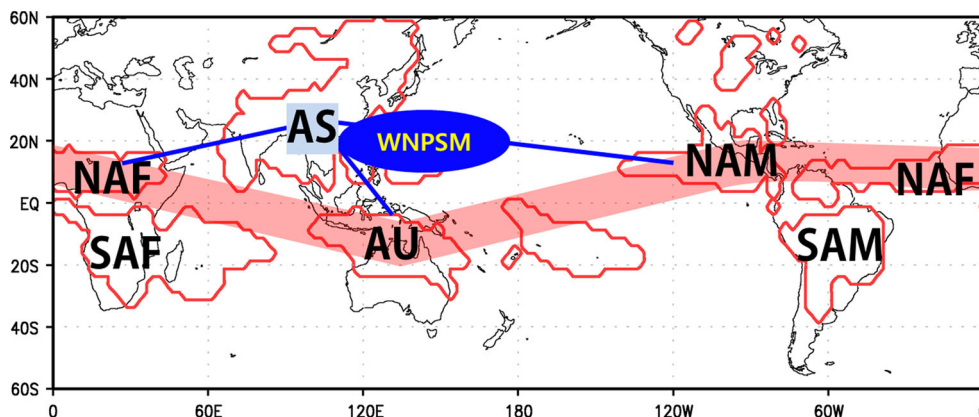

Fig. 6 Spatial patterns of first EOF mode of summer (JJA) precipitation over the AS domain during **a** P1 and **b** P2. Distributions of simultaneous correlation coefficients between the time series of PC1 and JJA SST anomalies during **c** P1 and **d** P2 are shown in *right pannels*. *Shading areas* in **c** and **d** denote regions significant at the 95 % confidence level

Sliding Corr between WNPMI and JJA SST anomaly

(a) 1986

(f) 1996

(b) 1988

(g) 1998

(c) 1990

(h) 2000

(d) 1992

(i) 2002

(e) 1994
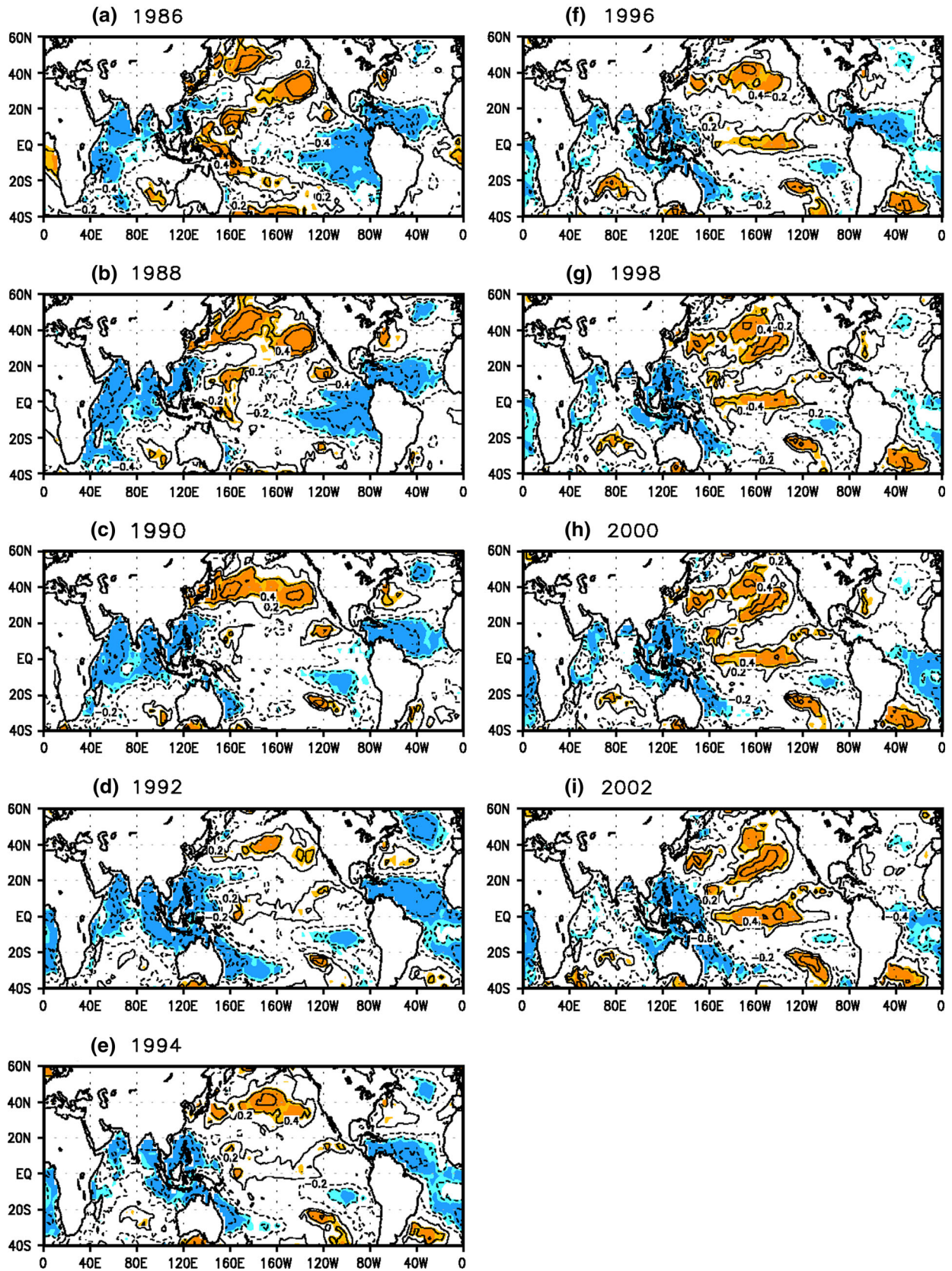
Sliding Corr between WNPMI and DJF SST anomaly

(a) 1986

(b) 1988

(c) 1990

(d) 1992

(e) 1994

(f) 1996

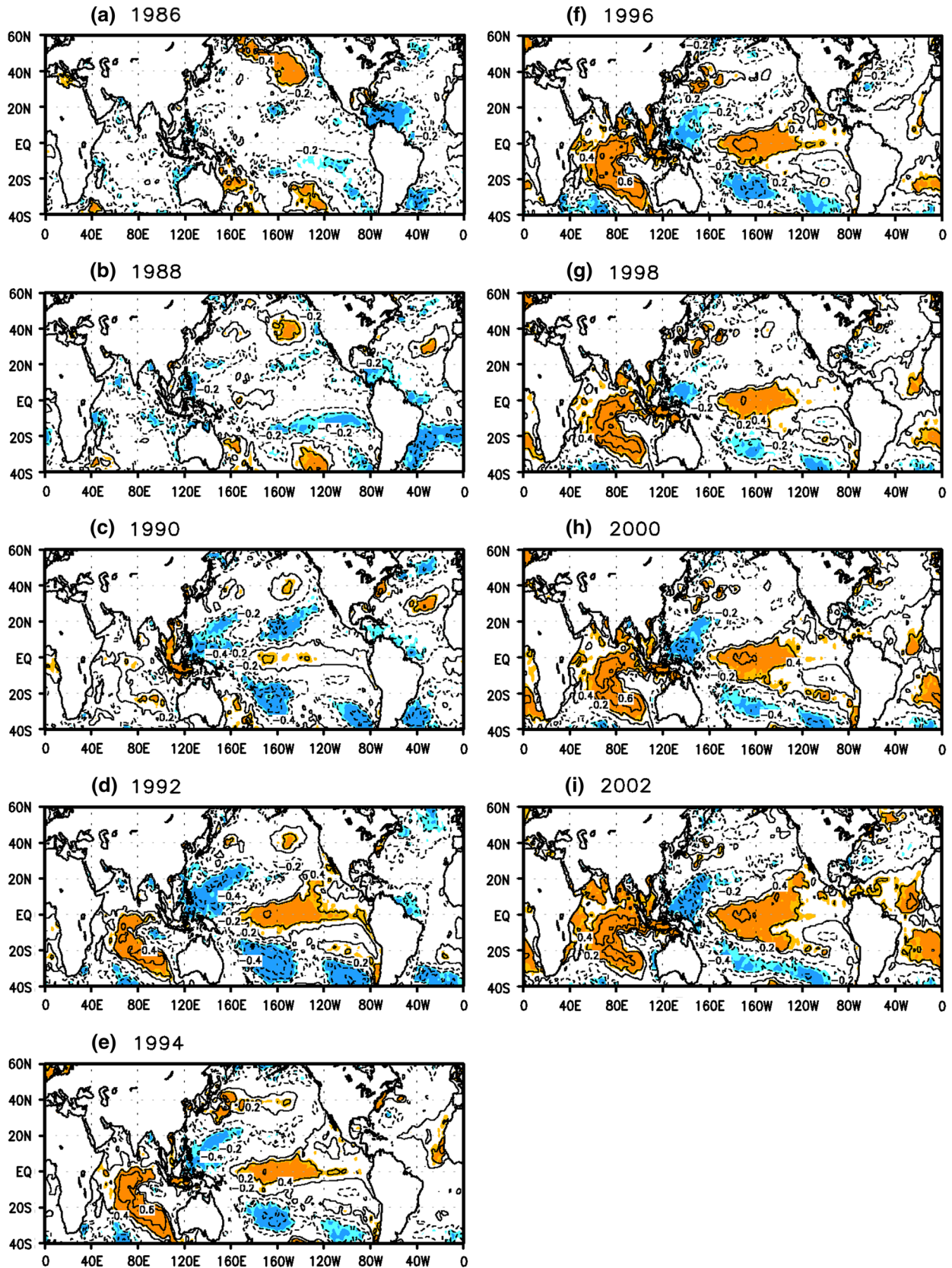

(g) 1998

(h) 2000

(i) 2002

◀**Fig. 8** Sliding correlations between the WNP summer monsoon precipitation index and the SST anomaly during the following winter (D(0)JF(+1)). The sliding window period is 15 years with the 2-year interval. *Year* of *each panel* indicates the central year of the window

These results appear to be related to different teleconnections of the EP–ENSO and the CP–ENSO with the Indian Ocean (Kao and Yu 2009).

Figure 9 shows the sliding correlation between the WNPSM and the geopotential height at 500 hPa. During P1, the WNPSM is linked to low latitudes. However, for P2 the relationship is weakened over the EP and a meridional wave train occurs from the WNP monsoon region. This wave train pattern is well matched with the low-level height anomalies and indicates a barotropic structure. However, a negative relationship is expanded from the WP to EP at 850 hPa (not shown), which implies that the WNPSM precipitation is closely related to the low-level height anomaly and the meridional pattern at the middle level.

To contrast characteristics between the EP cooling year and the CP warming year, the composite difference between EP cooling year during P1 and CP warming year during P2 is obtained (Fig. 10). For the EP cooling year during P1, 1984, 1985, 1988, and 1989 cases are selected. 1994, 1997, 2002, 2004, and 2009 cases are selected for the CP warming year during P2. The cyclonic circulation anomaly over the WNP region is strengthened in the CP warming case. These wind anomalies are related to the recent WNPSM and are expanded to the EP with strong easterly anomalies near the equator, which indicates that the CP warming is more strongly related to Pacific. Moreover, the difference map shows that the meridional wave train from the WNPSM region to the northern Japan as shown in Yun et al. (2008). This wave train is similar to the spatial distribution of correlation coefficient between the WNPSM and the height anomaly at 500 hPa.

4 Possible causes

4.1 Precipitation changes due to the oceanic forcing

To further reveal whether the interannual variation of summer precipitation significantly relates to ENSO, spatial distributions of the correlation coefficient between the observed summer SST anomalies and the PC time series of first mode (PC1) over the AS domain are investigated during P1 and P2 (Fig. 6c, d). During P1, the local SST anomalies and the PC1 are negatively correlated over the tropical eastern Pacific and positively correlated over the Western North and South Pacific Oceans. Thus, WNPSM precipitation is apparently related to the eastern Pacific (EP) cooling and the western Pacific (WP) warming. These

positive correlations also appear in the central mid-latitude Pacific of both hemispheres. The warmer waters wrapped in a horseshoe shape are located around the core of cooler than normal SST, which indicates a La Niña pattern. During La Niña summers, the NAM and NAF regions are cooler than normal. During P2, PC1 is positively correlated with summer SST anomalies over the central Pacific and negatively correlated over the Maritime Continent and southern Atlantic Ocean, which resembles the central Pacific (CP) El Niño related to subtropical Pacific and Asian–Australian monsoons.

The CP and EP El Niños were first introduced by Yu and Kao (2007) and Kao and Yu (2009) and the CP El Niño was named as El Niño Modoki (pseudo El Niño) by Ashock et al. (2007). According to them, generation mechanisms for CP El Niño differ from these for EP El Niño. Ashock et al. (2007) highlighted wind-induced thermocline variations in the tropical Pacific for the SST evolution and Kug et al. (2009) emphasized zonal advection in the ocean. Yu et al. (2011) indicated that the ocean advection is more important to the evolution of these nonconventional El Niño occurrences during its growth periods. As described previously, these changes in SST patterns related to the AS monsoon precipitation can affect the global monsoon.

4.2 Effects of SST forcing over EP and CP

We found that the WNPSM is related to EP cooling and CP warming during P1 and P2 in the observation data. Prior to examining the impact of the SST forcing over the EP and the CP, we have conducted the composite analysis of the observed 850-hPa geopotential height anomaly and surface (Fig. 10) to compare properties of EP cooling and CP warming. The composite difference result confirms that the effects of the EP cooling and the CP warming differ distinctly each other. When the average of normalized SST anomaly over the EP (CP) is less (greater) than -0.5 (0.5) during P1 (P2), the year is selected as a case of EP cooling (CP warming). Four or five cases are selected as the composite for negative (cold) EP SSTs and positive (warm) CP SSTs, respectively. Figure 10 shows composite differences between EP cooling and CP warming. Over the WNPSM region, a significant cyclonic circulation occurs in addition to significant negative height anomalies over the tropical and southern Pacific Ocean. A meridionally propagating wave train appears from the WNP to Japan, which resembles the spatial pattern of the strong WNPSM features suggested by Wang et al. (2001). Contrasting the strong WNPSM and this composite difference, some differences in the teleconnection appears over northern United States.

The model experiments are driven by climatological SST with only seasonal cycle. After a 20-year integration,

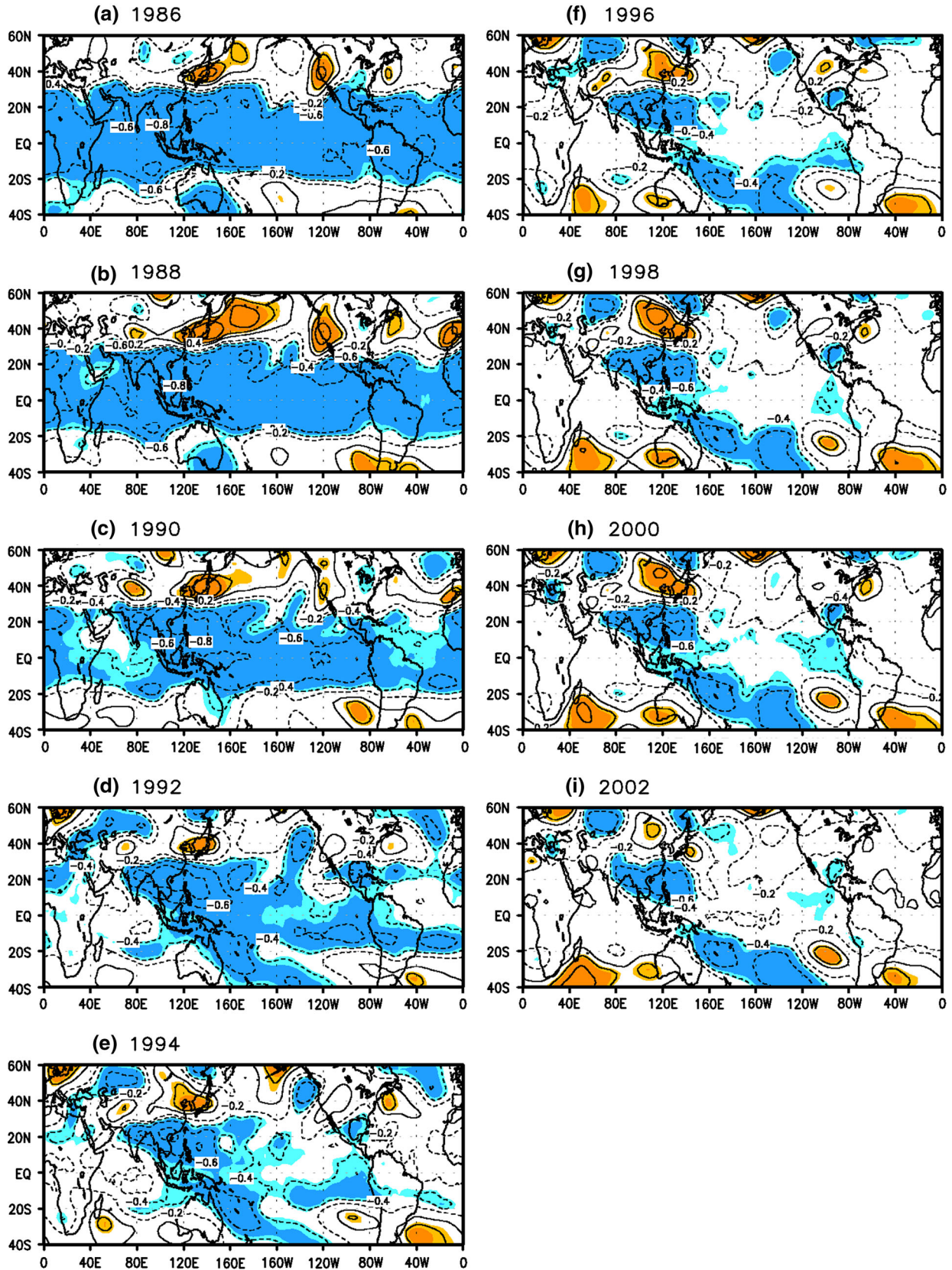Sliding Corr between WNPMI and JJA H500 anomaly

(a) 1986 (f) 1996
(b) 1988 (g) 1998
(c) 1990 (h) 2000
(d) 1992 (i) 2002
(e) 1994

the results from the last 15 years of the simulation are considered. The EP and CP SST forcings are specified by doubling the composite of the observed SST values. We conducted a set of four ensemble experiments. For the eastern Pacific cooling (EPC_P1) forcing, spatial-averaged SST anomalies in the eastern Pacific region (10°S–10°N, 160°E–80°W) which is less than −0.5 are summed and divided number of cases during P1. For the central Pacific warming (CPW_P2) forcing, the same method is applied but for the average is greater than 0.5 in the central Pacific region (10°S–10°N, 160°E–100°W) during P2. This set of experiments is expected to reveal the different effects of SSTs over the EP and the CP, which are shown by black dashed contours in Figs. 11b and 12b, respectively.

The EP cooling and the CP warming forcings are prescribed by doubling the composite anomalies of the observational SST data. The results of two experiments for the precipitation and the geopotential height at 850 hPa during the summer are shown in Figs. 11 and 12. The differences in the vertical velocity as omega, precipitation, and 850-hPa geopotential height between the EPC_P1 and the CTL_P1 are shown in Fig. 11. The omega response, which is the value multiplied by -1, of the EP cooling results in a slightly descending motion over the equator and a decrease in precipitation compared to the CTL_P1. With the EP cooling forcing, suppressed convection is revealed over the north of the equator because SST cooling is a stronger forcing during the summer than the winter. Also, this forcing weakens precipitation near the NAM. Also, the cyclonic circulation and summer precipitations over the WNP monsoon region are appeared, when SSTs are cooler than normal over the EP.

From the differences between the CPW_P2 and the CTL_P2, we found that the CP warming forcing (Fig. 12) causes a more active response vertically than the EP cooling forcing does. The SST warming forcing simulates stronger ascending motions over the warming forcing region compared with CTL_P2. The strong convection over the warming region causes an increase in precipitation. Near the CP warming region, the strong convection induces the low pressure and the convergence. According to the air–sea interaction reported by Wang et al. (2000), the in situ air–sea interaction in the WNP cyclone plays a key role in the bonding of the equatorial CP cooling and strong East Asian winter monsoon. Such a connection differs from this study because this mechanism is related to the winter monsoon. A strong WNPSM occurs in the decay phase of ENSO cool episodes. This mechanism can explain the relationship between EP cooling and WNPSM precipitation during P1. A cyclonic circulation over the western part of the warming occurs, and the convergence to this warming is added to the mean trade wind, which creates a small cyclonic circulation over the WNP. This small cyclonic circulation leads to the increasing precipitation over the WNP. This model has some biases. The precipitation region over the WNP is located to the south. However, we argued that the cyclonic circulation was more dominant during CP warming cases than during EP cooling cases through the model experiment and the composite analysis. Moreover, decreases in precipitation over the NAF and the NAM appeared. The decrease over both the NAF and the NAM and the increase over the WNP well match with the changes in interrelationships of regional monsoon precipitations founded in observational data.

5 Summary and discussion

This study aims to examine the interdecadal and the interannual variability of global monsoon precipitation. As

Fig. 10 The composite difference between EP cooling cases during P1 and CP warming cases during P2. The *contour* represents the geopotential height at 850 hPa and the *shaded area* means significant values at the 95 % confidence level. *Arrows* are surface wind vectors significant at the 95 % confidence level
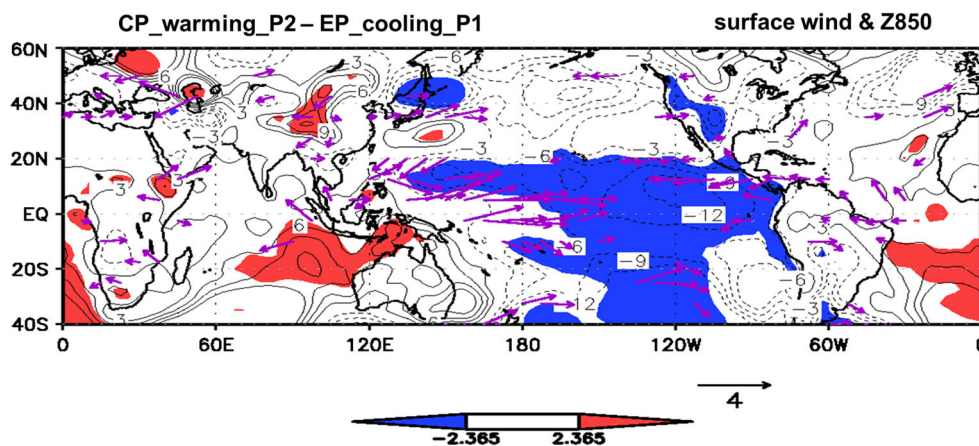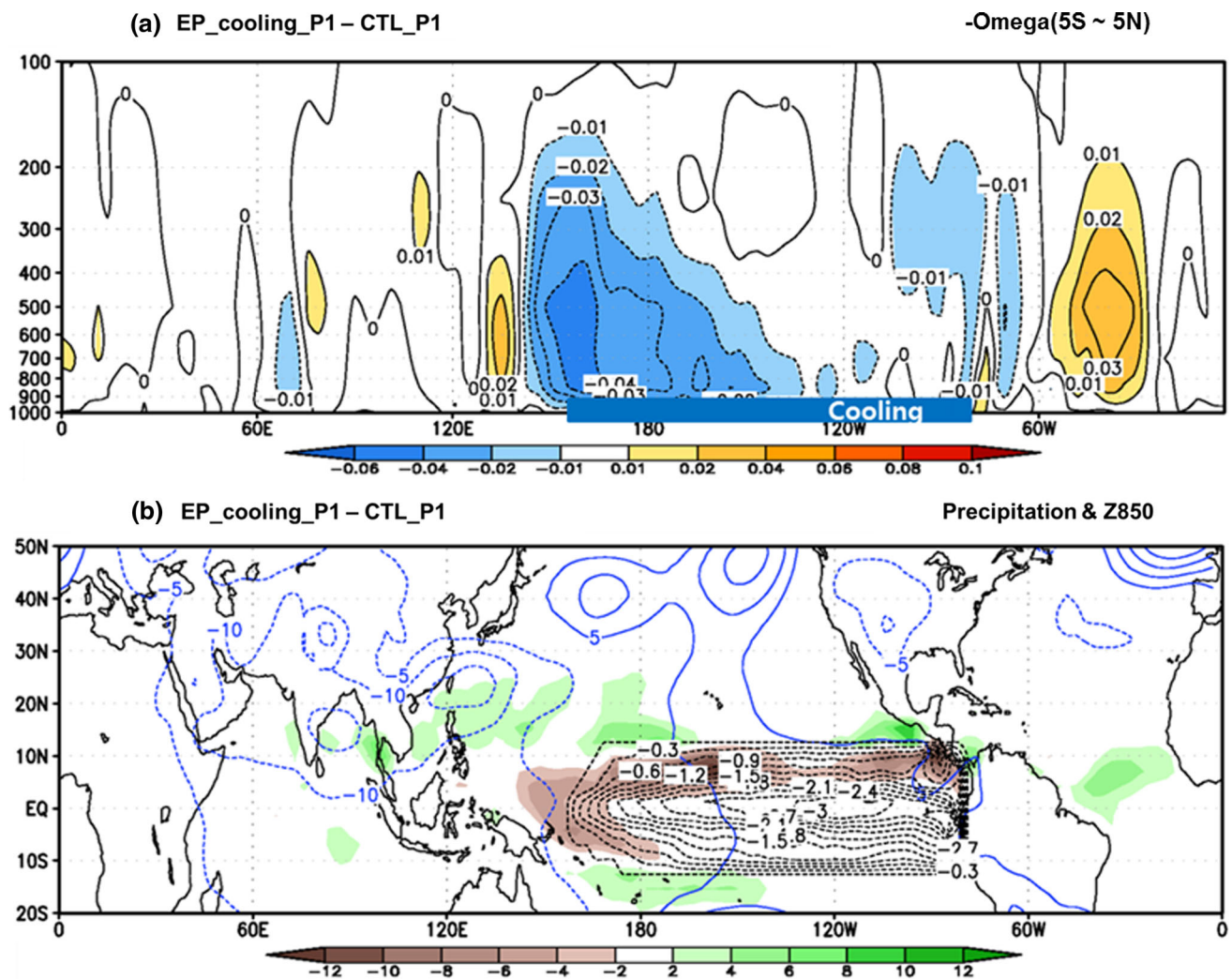
Fig. 11 The difference between EPC_P1 and CTL_P1 for **a** omega averaged from 5°S to 5°N and **b** precipitation and geopotential height at 850 hPa during the boreal summer. The cooling region is denoted by a *shaded box* in **a** and *black contours* in **b**. The *blue contour* and *shading area* in **b** indicate geopotential height at 850 hPa and precipitation, respectively. *Black dashed lines* in **b** indicate the SST forcings over the EP (10S–10N, 160E–80W) cooling used in experiments of ECHAM 4.6 model

defined by Wang and Ding (2006), six global monsoon domains are used. The interdecadal variability of GM has an increasing trend for AR and the summer, which indicates that the global summer monsoon is gradually intensified. Moreover, this interdecadal variability is related to the positive phase of IPO. In a large scale, SSTs are assumed to be dominant drivers for interdecadal changes in global monsoons.

The interannual variations of GM and SH monsoon domains show no remarkable changes. On the contrary, interannual variability of precipitation over the NH monsoon domain is weakened during the recent decade. By using two tests for change-point detection, the year of 1993 is found as a change-point. The entire period may be divided into P1 and P2 subperiods. A comparison of P1 and

P2 reveals changes in relationships among regional monsoon precipitations. During P2, NAM and NAF over the NH and AU over the SH are positively correlated one another, and all three regional monsoons are negatively related to the AS monsoon. The sudden weakening of summer precipitation over the NH could be caused by the cancellation of regional monsoon precipitation.

The most dominant pattern of precipitation over the AS monsoon domain is changed from an ENSO-related mode to a WNPSM-related mode. In addition, the ENSO-related mode shows a negative correlation with SSTs over the EP (EP-cooling mode) during P1. The WNPSM-related mode exhibits a positive correlation with SSTs over the CP (CP-warming mode). The SST pattern related to the AS monsoon is changed from EP cooling to CP warming. Three
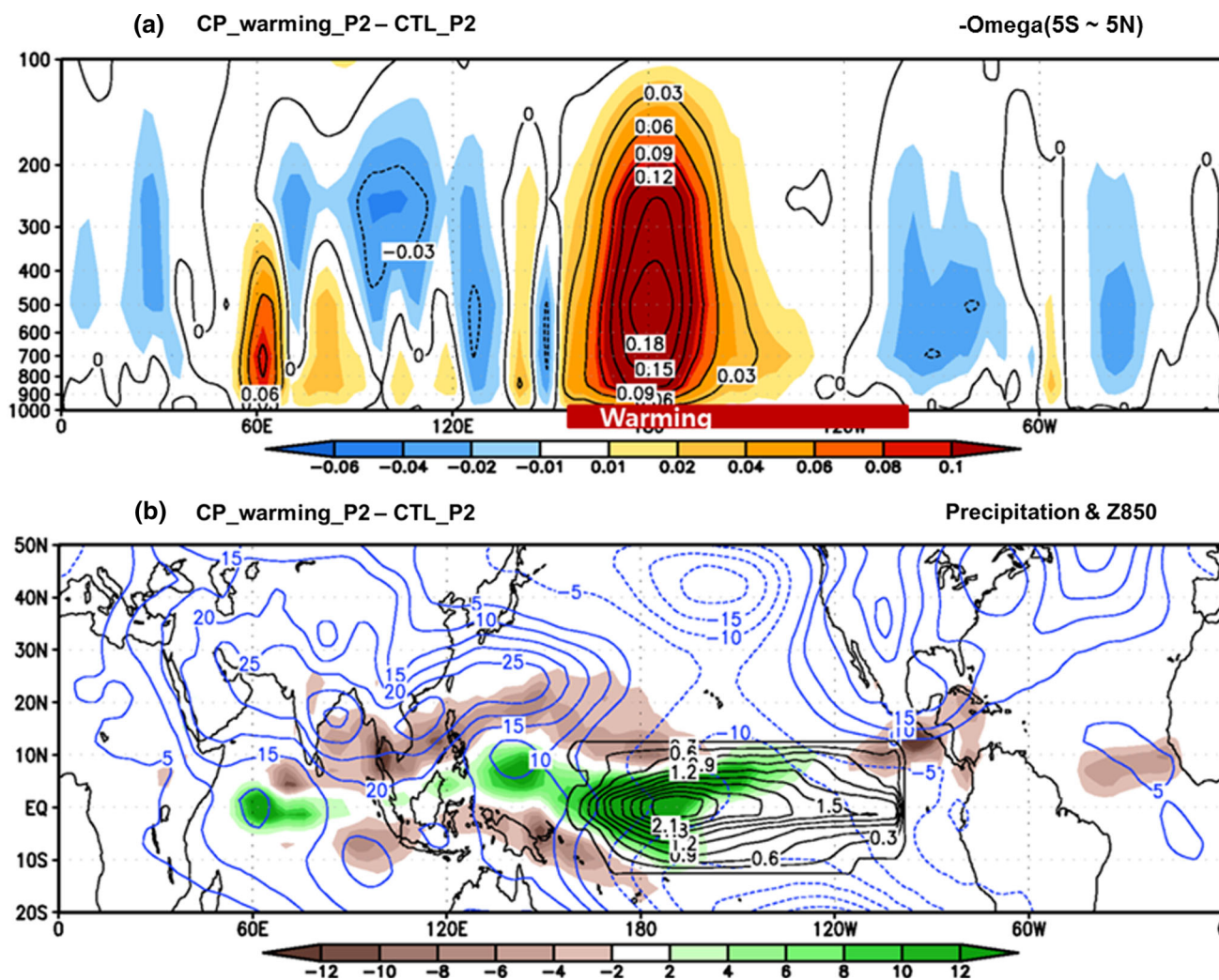
Fig. 12 The difference between CPW_P2 and CTL_P2 for **a** omega averaged from 5°S to 5°N and **b** precipitation and geopotential height at 850 hPa. The warming region is denoted by a *shaded box* in **a** and *black contours* in **b**. The *blue contour* and *shading area* in **b** indicate the geopotential height at 850 hPa and precipitation, respectively. *Black solid lines* in **b** indicate the SST forcings over the CP (10S–10N, 160E–100W) forcing used in experiments of ECHAM 4.6 model

Fig. 13 The schematic diagram of responses for the CP warming
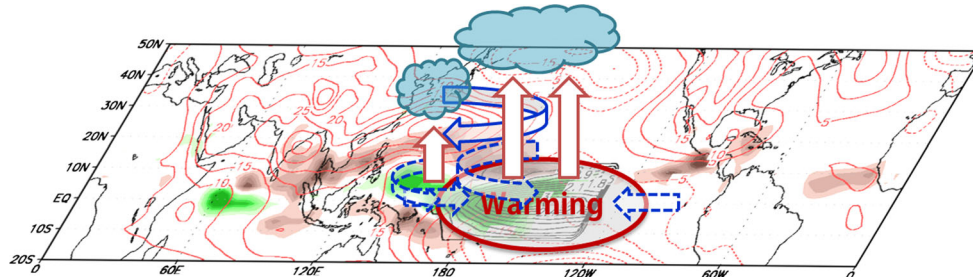
regional monsoon domains (ID, EA, and WNP) belong to the AS monsoon domain, and the WNP mainly contributes to the AS monsoon. Therefore, the WNPSM may be a key factor in changes in global monsoon relationships.

The composite difference for meteorological fields between the EP cooling year and the CP warming year shows a suppressed convection over the WNPSM region and the equatorial Pacific. Moreover, a meridional wave train appears from the WNPSM region to the northern Japan. Over the WNP monsoon region, a cyclonic circulation anomaly is dominant in P2, which is added to the equatorial easterlies in the CP.

In model experiments, both the EP cooling and the CP warming forcings simulates effectively the precipitation

over the WNP. In addition, a negative relationship among the three types of NH monsoon precipitation appears in the CP warming forcing experiment. A schematic diagram of responses for the CP warming is shown in Fig. 13. In the warming region, a convergence is formed, and an active convection is created by this convergence. A cyclonic circulation is formed in the western edge of the warming region. In term of the CP warming, the WNP summer monsoon plays a key role that causes changes in relationships among global monsoon precipitation. It is consistent result with recent study. Wang et al. (2013) demonstrated that the western Pacific subtropical High variation is primarily controlled by central Pacific cooling/warming and a positive atmosphere–ocean feedback between the western Pacific subtropical high and the Indo-Pacific warm pool oceans.

Wu et al. (2009, 2010) suggested that both the tropical Indian Ocean and the western Pacific SST anomalies play dominant roles in the maintenance of the western Pacific anticyclone in El Nino-decaying summer. In this study, SST anomalies are prescribed only over Pacific. For further experiment, we need to consider the IO and the WNP SST anomalies.

Appendix: Change-point detection methods

In this study, two methods were used for change-point detection. The Lepage test (Lepage 1971; Yonetani and Gregory 1994) is a non-parametric test that investigates significant differences between two samples, even if the distributions of the parent populations are unknown. The Lepage statistic, HK (symbol used by Yonetani and Gregory 1994), is combination of standardized statistics of Wilcoxon and Ansari-Bradley (Lepage 1971). If HK is greater than 5.99 or 9.21, the mean change between the two samples is significant at the 95 or 99 % confidence level, respectively.

The second methods is the Pettitt test (1979, 1980a). Pettitt derived the test statistic on the basis of changes in the median of the observation sequence by examining the rank of the observations. The Pettitt test uses a remarkably stable distribution and provides a stout test of the change-point resistant to outliers (Pettitt 1980b). The Pettitt test procedure is as follows:

First, each of the observations $X_1, X_2, \ldots, X_N$ is ranked from 1 to N. Let r_i be the rank associated with the observations X_i. Then, at each place j in the series, we calculate

$$W_j = \sum_{i=1}^{j} r_i, \quad j = 1, 2, \ldots, N-1, \quad (1)$$

which is the sum of the ranks of the variables at or before point j. Next, for each point in the sequence, we calculate $2W_j - j(N+1)$ to set

$$K_{m,n} = \max |2W_j - j(N+1)|, \quad j = 1, 2, \ldots, N-1. \quad (2)$$

The value of j where the maximum in $K_{m,n}$ occurs is the estimated change-point in the sequence and is denoted by m. The number of observations after the change-point is $n = N - m$. The sampling distribution of W_m is normally distributed with mean $m(N+1)/2$ and variance $mn(N+1)/12$ when N is large. We then perform a statistical test to determine whether the estimated change-point m is significant by using the sampling distribution of W_m.

References

Adams DK, Comrie AC (1997) The North American monsoon. Bull Am Meteorol Soc 78:2197–2213

Adler RF, Huffman GJ, Chang A et al (2003) The version 2 Global Precipitation Climatology Project (GPCP) monthly precipitation analysis (1979–present). J Hydrometeorl 4:1147–1167

Ashock K, Behera SK, Rao SA, Weng H, Yamagata T (2007) El Niño Modoki and its possible teleconnection. J Geophys Res 112:C11007

Chen J, Gupta AK (2000) Parametric statistical change point analysis. Birkhauser, Basel

Ha KJ, Ha E (2006) Climatic change and interannual fluctuations in the long-term record of monthly precipitation for Seoul. Int J Climatol 26(5):607–618

Hsu P, Li T, Wang B (2011) Trends in global monsoon area and precipitation over the past 30 years. Geophys Res Lett 38:L8701

Kalnay E, Kanamitsu M, Kistler R et al (1996) The NCEP/NCAR 40-year reanalysis project. Bull Am Meteorol Soc 77:437–471

Kao HY, Yu JY (2009) Contrasting eastern-Pacific and central-Pacific types of ENSO. J Clim 22:615–632

Kitoh A, H Endo, KK Kumar, IFA Cavalcanti, P Goswami, T Zhou (2013) Monsoons in a changing world: a regional perspective in a global context. JGR. doi:10.1002/jgrd.50258

Kug JS, Jin FF, An SI (2009) Two types of El Niño events: cold tongue El Niño and warm pool El Niño. J Clim 22:1499–1515

Kwon MH, Jhun JG, Wang B, An SI, Kug JS (2005) Decadal change in relationship between east Asian and WNP summer monsoons. Geophys Res Lett 32:L16709

Lee JY, B Wang (2012) Future change of global monsoon in the CMIP5. Clim Dyn. doi:10.1007/s00382-012-1564-0

Lepage Y (1971) A combination of Wilcoxson's and Ansari-Bradley's statistics. Biometrika 58:213–217

Li H, Zhou T, Li C (2010) Decreasing trend in global land monsoon precipitation over the past 50 years simulated by a coupled climate model. Adv Atmos Sci 27(2):285–292. doi:10.1007/s00376-009-8173-9

Liu J, Wang B, Ding Q, Kuang X, Soon W, Zorita E (2009) Centennial variations of the global monsoon precipitation in the

last millennium: results from ECHO-G model. J Clim 22:2356–2371

Pettitt A (1979) A non-parametric approach to the change-point problem. Appl Stat 28(2):126–135

Pettitt A (1980a) A simple cumulative sum type statistic for the change-point problem with zero-one observations. Biometrika 67:79–84

Pettitt A (1980b) Some results on estimating a change-point using nonparametric type statistics. J Stat Comput Simul 11:261–272

Rayner NA, Parker DE, Horton EB, Folland CK, Alexander LV, Rowell DP, Kent EC, Kaplan A (2003) Global analyses of sea surface temperature, sea ice, and night marine air temperature since the late nineteenth century. J Geophys Res 108:4407. doi:10.1029/2002JD002670

Roeckner E et al (2003) The atmospheric general circulation model ECHAM5, part I: model description. Max-Planck-Inst für Meteorol Rep 349:127

Trenberth K, Stepaniak D, Caron J (2000) The global monsoon as seen through the divergent atmospheric circulation. J Clim 13:3969–3993

Wang B, Ding Q (2006) Changes in global monsoon precipitation over the past 56 years. Geophys Res Lett 33:L06711

Wang B, Ding Q (2008) Global monsoon: dominant mode of annual variation in the tropics. Dyn Atmos Ocean 44:165–183

Wang B, Wu R, Fu X (2000) Pacific-east Asian teleconnection: how does ENSO affect east Asian climate? J Clim 13:1517–1536

Wang B, Wu R, Lau KM (2001) Interannual variability of the Asian summer monsoon: contrasts between the Indian and the western north Pacific-east Asian monsoons. J Clim 14:4073–4090

Wang B, Wu R, Li T (2003) Atmosphere-Warm ocean interaction and its impact on Asian-Australian monsoon variation. J Clim 16:1195–1211

Wang B, Yang J, Zhou T, Wang B (2008) Interdecadal changes in the major modes of Asian–Australian monsoon variability: strengthening relationship with ENSO since the late 1970s. J Clim 21:1771–1789

Wang B, Liu J et al (2012) Recent change of the global monsoon precipitation (1979–2008). Clim Dyn 39:1123–1135

Wang B, Xiang B, Lee JY (2013) Subtropical high predictability establishes a promising way for monsoon and tropical storm predictions. PNAS 110:2718–2722

Wu B, Zhou T, Li T (2009) Seasonally evolving dominant interannual variability modes of East Asian climate. J Clim 22:2992–3005

Wu B, Li T, Zhou T (2010) Relative contributions of the Indian Ocean and local SST anomalies to the maintenance of the western North Pacific anomalous anticyclone during El Niño decaying summer. J Clim 23:2974–2986

Yonetani T, Gregory JMC (1994) Abrupt changes in regional temperature in the conterminous United States, 1895–1989. Clim Res 4:13–23

Yu JY, Kao HY (2007) Decadal changes of ENSO persistence barrier in SST and ocean heat content indices: 1958–2001. J Geophys Res 112:13106

Yu JY, Kao HY, Lee T (2011) Subtropics-related interannual sea surface temperature variability in the equatorial central Pacific. J Clim 23:2869–2884

Yun KS, Seo KH, Ha KJ (2008) Relationship between ENSO and northward propagating intraseasonal oscillation in the east Asian summer monsoon system. J Geophys Res 113:D14120. doi:10.1029/2008JD009901

Yun KS, Seo KH, Ha KJ (2010) Interdecadal change in the relationship between ENSO and the intraseasonal oscillation in East Asia. J Clim 23:3599–3612. doi:10.1175/2010JCLI3431.1

Zhang L, Zhou T (2011) An assessment of monsoon precipitation changes during 1901–2001. Clim Dyn 37:279–296. doi:10.1007/s00382-011-0993-5

Zhang L, Zhou T, Wu B, Bao Q (2010) The annual modes of tropical precipitation simulated by the LASG/IAP coupled ocean-atmosphere model FGOALS_s1.1. Acta Meteorol Sinica 24(2):189–202

Zhou T, Zhang L, Li H (2008a) Changes in global land monsoon area and total rainfall accumulation over the last half century. Geophys Res Lett 35:L16707. doi:10.1029/2008GL034881

Zhou T, Yu R, Li H, Wang B (2008b) Ocean forcing to changes in global monsoon precipitation over the recent half-century. J Clim 21:3832–3852

Zhou T, Wu B, Scaife AA, Bronnimann S et al (2009) The CLIVAR C20C project: which components of the Asian-Australian monsoon circulation variations are forced and reproducible? Clim Dyn 33:1051–1068. doi:10.1007/s00382-008-0501-8

Zhou T, Hsu HH, Matsuno J (2011) Summer monsoons in East Asia, Indochina, and the western North Pacific. The global monsoon system: research and forecast, 2nd edn. World Scientific Publishing Co, Singapore, pp 43–72